Research Paper
J. Astron. Space Sci. 35(4), 211-218 (2018)
https://doi.org/10.5140/JASS.2018.35.4.211

JASS Journal of Astronomy and Space Sciences

Analysis of Solar Microwave Burst Spectrum, I. Nonuniform Magnetic Field

Jeongwoo Lee†
Institute of Space Sciences, Shandong University, Weihai, Shandong 264209, China

Solar microwave bursts carry information about the magnetic field in the emitting region as well as about electrons accelerated during solar flares. While this sensitivity to the coronal magnetic field must be a unique advantage of solar microwave burst observations, it also adds a complexity to spectral analysis targeted to electron diagnostics. This paper introduces a new spectral analysis procedure in which the cross-section and thickness of a microwave source are expressed as power-law functions of the magnetic field so that the degree of magnetic inhomogeneity can systematically be derived. We applied this spectral analysis tool to two contrasting events observed by the Owens Valley Solar Array: the SOL2003-04-04T20:55 flare with a steep microwave spectrum and the SOL2003-10-19T16:50 flare with a broader spectrum. Our analysis shows that the strong flare with the broader microwave spectrum occurred in a region of highly inhomogeneous magnetic field and vice versa. We further demonstrate that such source properties are consistent with the magnetic field observations from the Michelson Doppler Imager instrument onboard the Solar and Heliospheric Observatory (SOHO) spacecraft and the extreme ultraviolet imaging observations from the SOHO extreme ultraviolet imaging telescope. This spectral inversion tool is particularly useful for analyzing microwave flux spectra of strong flares from magnetically complex systems.

Keywords: microwave radiation, spectroscopy, electron acceleration, solar flares

1. INTRODUCTION

Solar microwave bursts provide information on high-energy nonthermal electrons accelerated using solar flares as a companion radiation source that shares the same diagnostic capability for electrons as hard X-rays and γ-rays (Kundu 1965; Brown 1973). In particular, solar microwave bursts under gyrosynchrotron radiation are emitted by keV to MeV electrons, accelerated during solar flares, perhaps via magnetic reconnection (e.g., Dulk & Marsh 1982; Dulk 1985; Kosugi et al. 1988). In comparison with hard X-rays that are accessible only from space observations, microwaves are accessible from ground-based observations (Zheleznyakov 1970; Melrose 1980). Another advantage is that microwave radiation depends not only on energetic electrons but also strongly on the magnetic field. As a result, microwave radiation can be more sensitive to a smaller number of electrons as long as there is sufficiently strong magnetic field in the source region. In spite of such observational advantages, microwave radiation has been less utilized for a couple of reasons. One reason is that the strong dependency on the magnetic field makes the inversion procedure more complicated because more parameters have to be considered in inverting the microwave spectrum than in extracting electron information from the hard X-ray spectrum. Nevertheless, many authors have conducted comparative studies on microwaves and hard X-rays to exploit the advantages of microwave radiation (Lee & Gary 1994, 2000; Holman 2003).

Many theoretical studies on gyrosynchrotron spectrum have been targeted to the coronal magnetic field embedded in source regions by inverting observed spectra (Benka & Holman 1992; Ai-hua & Karlický 1994; Nindos et al. 2000; Huang & Nakajima 2002; Gary & Hurford 2004; Kundu et al. 2004; Huang 2006; Nita et al. 2015; Casini et al. 2017; Kuroda et al. 2018). A full expression for the gyrosynchrotron

Received 29 NOV 2018 **Revised** 9 DEC 2018 **Accepted** 10 DEC 2018
†**Corresponding Author**
Tel: +86-631-5688881, E-mail: leej@sdu.edu.cn
ORCID: https://orcid.org/0000-0002-5865-7924

http://janss.kr pISSN: 2093-5587 eISSN: 2093-1409

emission is rather complicated (Ramaty 1969), and direct inversion to source properties is generally not possible. Typical inversion procedures often involve forward modeling in which we start from a set of prescribed values of the relevant parameters including magnetic field and adjust them by minimizing the difference between the calculated and the observed two-dimensional (2D) maps of microwave emission. Most of these models assume a uniform source. More recently, Moschou et al. (2018) used global simulations of three-dimensional (3D) MHD via the block-adaptive-tree-solarwind-roe-upwind-scheme (BATS-R-US) code (Powell et al. 1999) and performed ray tracing in 3D space. Otherwise, the inhomogeneous magnetic structure in the source has posed a problem in spectral inversions. In particular, some types of low-frequency microwave burst spectra, with fluxes much stronger than predicted by the homogeneous source mode, have been quite commonly found in the large database of the Owens Valley Solar Array (OVSA) by Lee et al. (1994) and the extended OVSA (EOVSA) by Kuroda et al. (2018). Other events of flat or extremely hard spectra have also been reported elsewhere (Raulin et al. 1999; Trottet et al. 2011; Song et al. 2016). Such non-standard spectral behavior makes interpretation of microwave burst spectrum more challenging.

In this paper, we present another inversion tool particularly designed to address the effects of inhomogeneous magnetic structure on solar microwave burst spectra. A unique feature of this new diagnostic tool is to treat the magnetic field as an independent variable spanning a wide range, while other approaches treat it as a single-valued parameter. The motivation is that the presence of nearly flat optically thick spectra indicates the radiative transfer along a wide range of magnetic fields, and as a result, the degree of inhomogeneity rather than a single value should be more important (Lee et al. 1994). Such inhomogeneity along the line of sight is an unavoidable issue in astronomical observations and cannot be directly addressed, even with imaging spectroscopy. We also challenge the traditional notion that the flux spectrum itself is much less informative than the intensity spectrum (Dulk 1985). An underlying idea is that the microwave source area can arbitrarily change with frequency. We argue that this is not the case, as the microwave source area may systematically vary with frequency given a magnetic field distribution. Moreover, to achieve a sufficient signal-to-noise ratio, a spatially-integrated flux spectrum is sometimes more desirable (Hwangbo et al. 2015). It is also true that integrated quantities, such as the total energy and particle number, are often more useful in characterizing the flare strength (Lee 2015). We present our new spectral analysis tool in Section 2 and the application results in Section 3. We validate the spectral analysis results in Section 4 and provide concluding remarks in Section 5.

2. BASIC IDEA AND FORMULATION

Unlike the solar hard X-ray burst spectrum, which is optically thin over the entire photon range, solar microwave spectrum often consists of both optically thin and thick regimes. The optically thin regime has a spectral slope mainly determined by the electron distribution in phase space and can be used for diagnosing electrons, like the hard X-ray spectrum (Brown 1973). It is the optically-thick regime where the microwave spectrum differs from the hard X-ray spectrum, and care must be taken for proper interpretation (Dulk 1985). The optically-thick spectrum is associated with the mean energy, and it represents the temperature for thermal electrons, with a spectral slope of 2, according to Kirchhoff's law of thermal radiation. For nonthermal relativistic electrons, it is closer to 2.5, according to analytic approximation (Rybicki & Lightman 1985). For mildly relativistic electrons, it may increase up to 2.9, according to the numerical approximation (Dulk & Marsh 1982). These simple relations are, however, valid only for homogeneous sources. For realistically inhomogeneous microwave sources, the optically-thick gyrosynchrotron spectrum can more slowly vary with frequency, as demonstrated by Lee et al. (1994), who adopted a 3D magnetic dipole model. Source inhomogeneity may be present not only on the projected sky-plane but also along the line of sight. The former effect can be addressed by imaging spectroscopy but not the latter; it is an unavoidable problem in all astronomical observations.

Our simple strategy for accommodating such magnetic inhomogeneity was to express the inhomogeneous 3D magnetic field distribution as a collection of multiple homogeneous sources, with its own cross section and thickness. Specifically, we expressed the source area, A, on the projected sky-plane and its thickness, L, along the line of sight in the form of scaling laws of magnetic field, B, as:

$$A_i = A_0 \left(\frac{B_i}{B_0}\right)^{-\alpha}, \quad L_i = L_0 \left(\frac{B_i}{B_0}\right)^{-\beta} \tag{1}$$

Here, index i, represents the number of individual model components, which was taken as seven in this study. B_0 should be sufficiently low, which was taken as 10 G in this study. B_6 is the highest field strength in the source, not exceeding the one measured in the photospheric magnetogram. With α and β, we manipulated how fast the area and thickness vary with magnetic field, depending on which the microwave flux from each of the seven

homogeneous components varies relative to each other. This is equivalent to decomposing the total volume of the source into a set of isogauss volume elements with different cross sections and thicknesses.

This technique was once used by Hwangbo et al. (2014) in an ad hoc manner, without proper introduction of the basic ideas. Fig. 1 illustrates how the scaling laws are used to control the resulting spectral morphology. Here, the symbols are the target microwave spectrum, which are actual OVSA data obtained for the October 19, 2003 flare at 16:51:56 UT. A total of 36 combinations of the two parameters, α and β, are displayed in such a way that α increases from left to right and β increases from top to bottom. For each combination of α and β, we adjusted A_0 and L_0 to achieve the closest fit to the target spectrum. The optically-thin spectrum (given by the points at frequencies higher than the peak frequency) is solely determined by the electron energy distribution and could immediately be fitted. This figure shows that the spectral slope (red lines) of the optically-thick spectrum (given by the points at frequencies lower than the peak frequency) systematically changes with α and β. Higher α corresponds to a larger weak-field source area. This boosts the low-frequency side of the flux spectrum. The other power-law index, β, plays a similar role in that higher β corresponds to a longer region filled with weaker field along the line of sight. For the extreme condition of inhomogeneity, for instance, $\alpha \geq 1.0$ and $\beta \geq 0.5$, we have an optically-thick spectrum that is nearly flat or even decreases with frequency, which is adequate for explaining unusual spectra (Raulin et al. 1999; Trottet et al. 2011; Song et al.

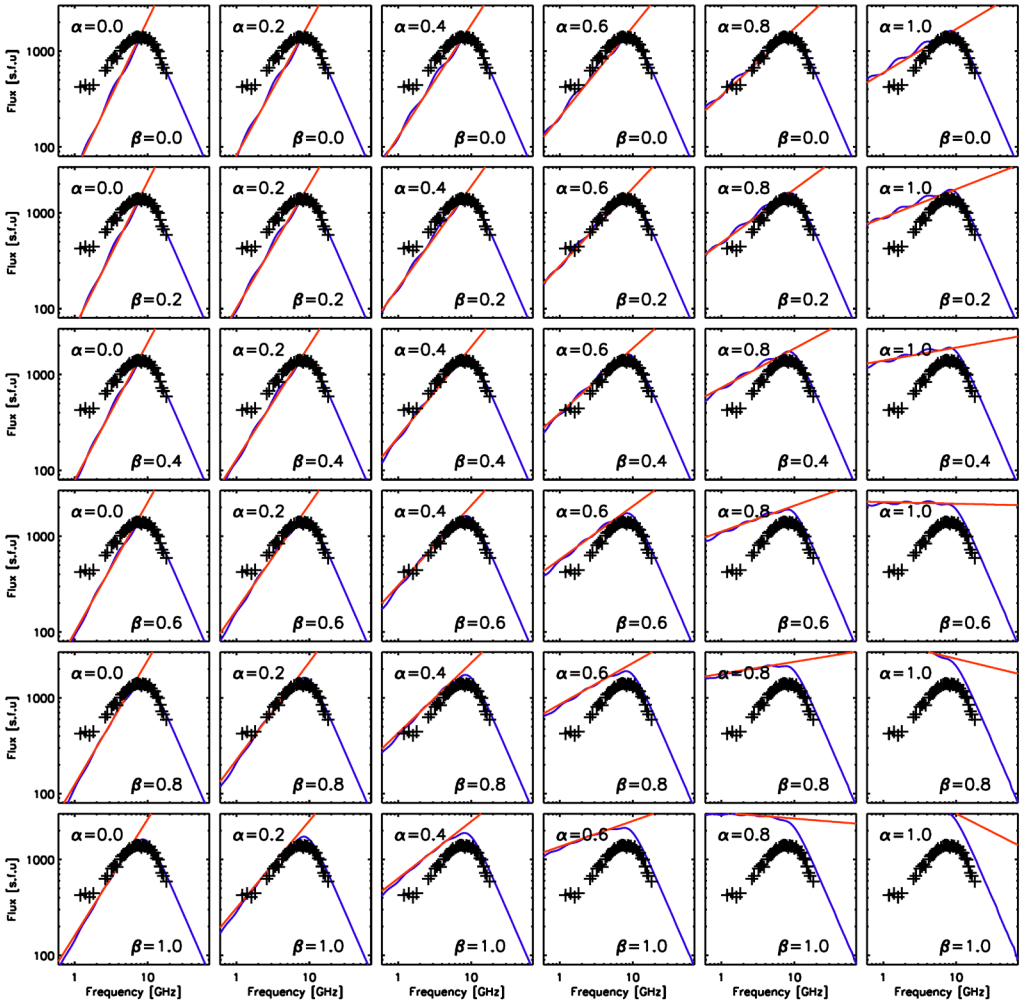

Fig. 1. The proposed spectral fitting procedure. A total of 36 model spectra (blue curves) calculated with a set of α and β are compared with the observed target spectrum (plus sign symbols). Models are arranged so that α increases from left to right, and β increases from top to bottom. For each combination of α and β, we adjust A_0 and L_0 to make the model most agreeable to the target spectrum. The optically-thin spectrum is immediately fit with the best matching electron energy distribution. The spectral slope of the optically-thick spectrum (red lines) has a systematic dependence on either α or β, which is used to make the spectral fit rapidly.

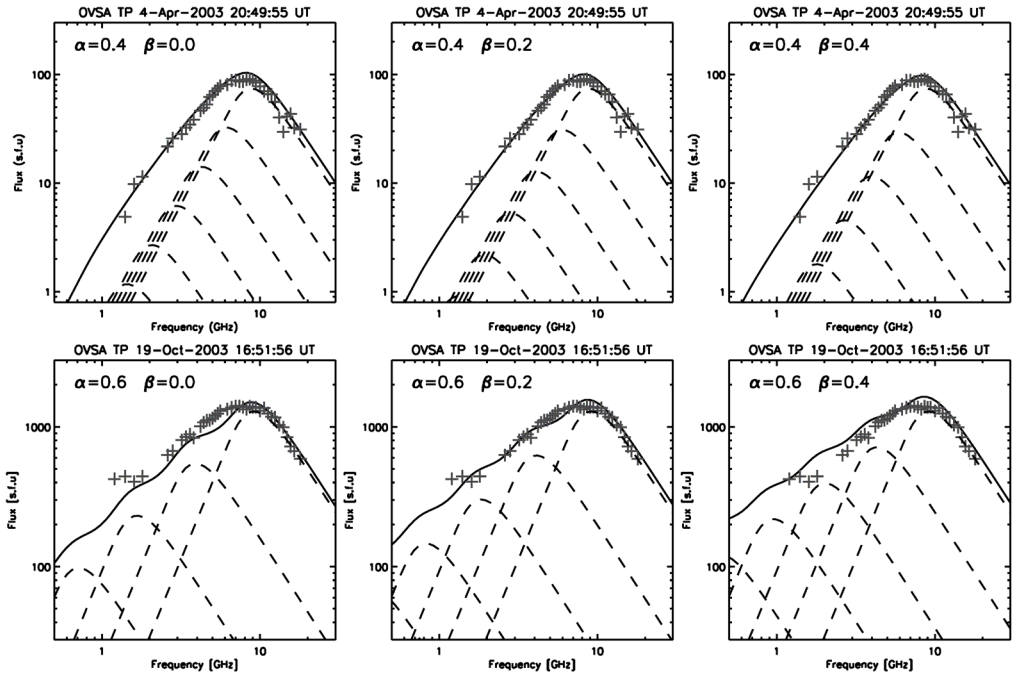

Fig. 2. Spectral fitting procedure. Symbols are the OVSA spectra taken as a target. Model fits using three combinations of α and β (solid lines) are shown for SOL2003-04-04T20:55 (top panels) and SOL2003-10-19T16:50 (bottom panels). The plus sign symbols are the OVSA spectra at the maximum phase of each event. Dashed lines represent the individual components of the microwave source obeying the scaling laws in Eq. (1)

2016). In the present case, the best fit was obtained with $\alpha \approx 0.6$ and $\beta \approx 0.2$, which defines the degree of unresolved magnetic field inhomogeneity in the present model setup.

3. SPECTRAL ANALYSIS OF OVSA DATA

We applied the above diagnostic procedure to two contrasting OVSA events of solar microwave bursts—SOL2003-04-04T20:55 (GOES class C9.0) and SOL2003-10-19T16:50 (GOES class X1.1) events—and present the OVSA data and spectral analysis in Fig. 2. Top panels show the OVSA total power spectrum (plus sign symbols) and analysis results obtained for the SOL2003-04-04T20:55 (GOES class C9.0) event. We note that this event is currently not listed in the GOES flare list, perhaps because it occurred at the end of the larger flare, SOL2003-04-04T20:19 (GOES class M1.9). Nevertheless, we regard it as a secondary flare event in the decay of the larger preceding flare, significant in microwave lightcurves. According to the OVSA database, this microwave burst started at 20:42:19 UT, peaked at 20:49:47 UT, and ended at 21:08:43 UT, with a peak flux, 97 s.f.u., at 7.6 GHz. The bottom panels of Fig. 2 show the SOL2003-10-19T16:50 flare. This strong X1.1 class flare started at 16:38:04 UT, peaked at 16:43:34, ceased at 17:09:16 UT, and exhibited a maximum flux of 1442 s.f.u. at 7.9 GHz. Not only the flux level but the overall spectral morphology makes a good contrast—the C9.0 flare has narrower spectra than the X1.1 flare overall. For the C9.0 flare, the OVSA total power spectrum (symbols in the top panels) has a low-frequency side spectral slope close to 2, implying that the source is likely to be relatively homogeneous. The spectrum for the X1.1 flare has a spectral slope much lower than 2, which implies that a highly inhomogeneous source is involved with the microwave bursts (cf. Lee et al. 1994).

We display the fitting results at three combinations of α and β for each event. For the C9.0 flare (top panels), a relatively low value of $0.35 \le \alpha \le 0.45$ is found to be appropriate, which indicates that the source area is relatively independent of magnetic field strength in our model setup. It seems that β plays a minor role, since the source area is already insensitive to magnetic field. Note, however, that even such a textbook-like spectrum with the spectral slope close to 2 needs some degree of inhomogeneity to make a perfect spectral fit. For the X1.1 flare (bottom panels), the spectral fit requires higher values of $0.5 \le \alpha \le 0.7$ and $0.1 \le \beta \le 0.3$. In this case, β does play a role. Overall, however, β turns out to be low, always below 0.3, which means that the variation in the source thickness of the magnetic field is less significant than that of the source area. It may be that the microwave source is relatively confined in height. Higher α for the X1.1 flare is expected because a large flare tends to occur in a magnetically complex

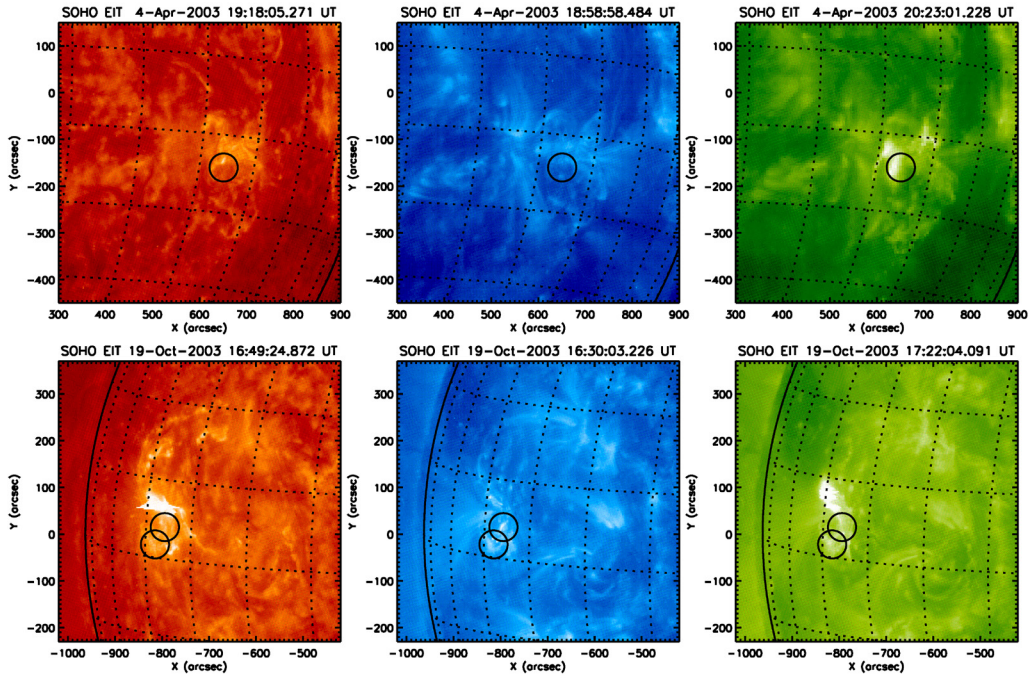

Fig. 3. SOHO's EIT images of the active regions that produced the two microwave bursts under study: NOAA AR 10324 located at S11W40 for the SOL2003-04-04T20:19 event (top panels) and NOAA AR 10484 located at N08E58 for the SOL2003-10-19T16:50 event (bottom). The black circles represent the locations of the 6–12 keV RHESSI sources reconstructed by the CLEAN algorithm, which are tentatively assumed to coincide with those of the microwave sources.

region. A higher value of α also implies that the energetic electrons access a significant portion of the weak-field region, as expected when the flare energy released is transported to a larger volume, spanning a wider range of magnetic field strength. Based on this spectral analysis, we conclude that the SOL2003-04-04T20:55 (GOES class C9.0) event is from a nearly homogeneous and compact source, and the SOL2003-10-19T16:50 event is from a highly inhomogeneous and extended source.

4. VALIDATION OF THE SPECTRAL ANALYSIS RESULTS

As a way to validate the spectral analysis results, we investigated the magnetic field and temperature structures using the extreme ultraviolet (EUV) images from the Solar and Heliospheric Observatory (SOHO) extreme ultraviolet imaging telescope (EIT) in Fig. 3 and the line-of-sight magnetograms around the source active region (AR) from the SOHO/Michelson Doppler Imager (MDI) magnetograms in Fig. 4.

4.1 EIT Images

Fig. 3 shows the EUV images at three wavelengths 304 Å, 171 Å, and 195 Å, which have the following properties. AIA 304 Å is emitted by He II at around 50,000 K from the chromosphere and transition region, showing footprints of relatively small loops. AIA 171 Å is emitted by Fe IX at around 0.6 MK and is the best wavelength for displaying coronal loops. AIA 193 Å is emitted by Fe XII at 1 MK and Fe XXIV at 20 MK. The former represents a slightly hotter region of the corona, and the latter represents the much hotter material of a solar flare. As can be seen in the figure, the SOL2003-04-04T20:55 flare occurred in NOAA AR 10324 at S11W40, relatively closer to the solar disk, and the SOL2003-10-19T16:50 occurred in NOAA AR10484, located at N08E58 at the time of flare, close to the eastern limb. The black circles show the locations of the 6–12 keV hard X-ray sources obtained from the *Reuven Ramaty High Energy Solar Spectroscopic Imager* (RHESSI, Lin et al. 2002). We tentatively assume that the locations of these X-ray sources should coincide with those of the microwave sources. The locations and sizes are taken from the RHESSI Quicklook Plots available from RHESSI Browser 2.0.

For the SOL2003-04-04T20:55 event, the RHESSI source at 6–12 keV is roughly a circle centered at (651″,–160″) at the time interval of 20:47:48 UT–20:48:00 UT. The EUV images show that the flare energy release is confined to a small region in the AR, although the entire AR is more complex. As a consequence, the microwave source is likely to be

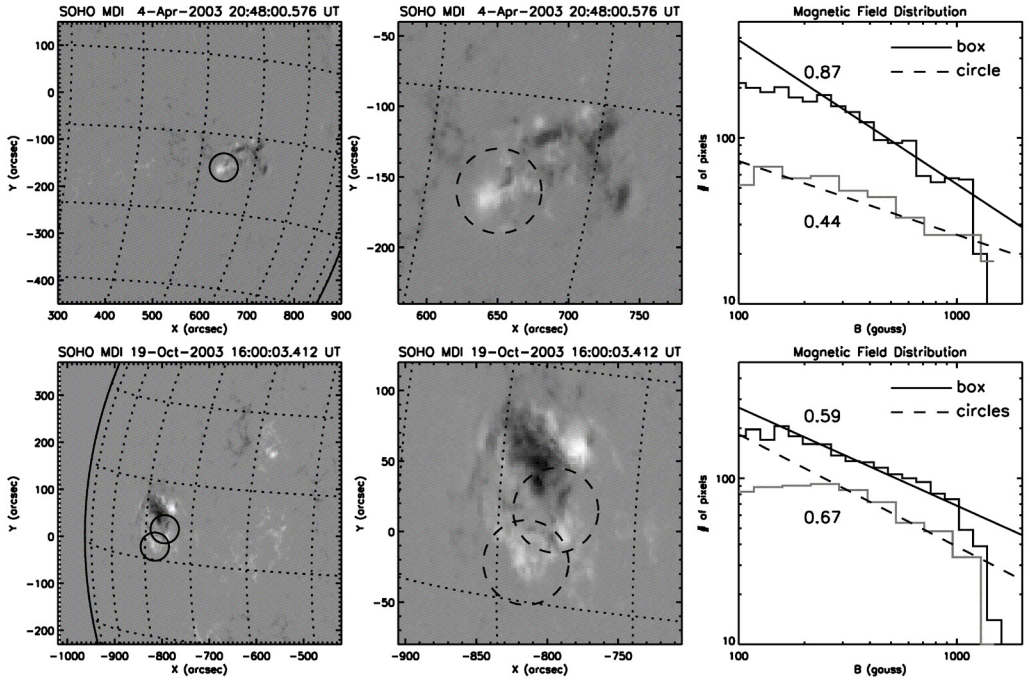

Fig. 4. SOHO/MDI magnetograms and the statistical distribution of the magnetic field in the source ARs, NOAA AR 10324 for the SOL2003-04-04T20:19 flare (top panels) and NOAA AR 10484 for the SOL2003-10-19T16:50 flare (bottom). The magnetograms in the left column have the same FOV as in Fig. 3, and those in the middle column show the close-up views of the ARs in 100″ × 100″ FOV. The black circles indicate the locations of the 6–12 keV RHESSI sources as in Fig. 3. The plots in the right column show the number of pixels arranged according to their field strengths. The fit to the power-law distributions are shown as solid lines (entire FOV in the middle panels) and dashed lines (circled regions only), with the power-law indices denoted for each fit.

embedded by relatively homogeneous fields, which is in agreement with the low value of $\alpha \approx 0.4$ found in the above spectral modeling. For the SOL2003-10-19T16:50 flare, two strong RHESSI sources appear in the core of the complex active region. This flare was well observed by SOHO/EIT, Transition Region and Coronal Explorer (TRACE), and Large Angle and Spectrometric Coronagraph (LASCO) to have very impulsive EUV emissions that are eruptive in nature. The EIT images at a larger field-of-view (FOV) show a coronal hole north of the AR and nearby active regions at its south, and this event was accompanied by a narrow coronal mass ejection. The EUV images here reveal a large magnetic loop connecting the two spots, in which case the energetic electrons can access a wide range of magnetic field regions (Lee 2004). This result is consistent with a high degree of magnetic field inhomogeneity, $\alpha \approx 0.6$, as found in the present spectral analysis of the OVSA data.

4.2 MDI Magnetograms

Fig. 4 shows the magnetic properties of the microwave burst sources using the SOHO/MDI magnetograms. Again, the data for the C9.0 flare are displayed in the top panels, and those for the X1.1 flare are displayed in the bottom panels. The panels in the leftmost column show the line-of-sight MDI magnetograms in the same FOV as that of Fig. 3, and those in the middle panels are the close-up views of the source ARs within the 100″ × 100″ FOV. The rightmost column shows the total pixel numbers containing the field strength in each preset interval so that it works as a proxy for the differential area as a function of magnetic field strength, as in Eq. (1). We must note that the magnetic field information that we inferred from the OVSA microwave spectrum pertains to the coronal source rather than the photospheric footpoints. It is tentatively assumed that the statistical property of magnetic field distribution would remain similar at different heights. The pixel counting was performed in the entire FOV of the middle panel (black histograms) and only for the circled regions centered at the RHESSI source (gray histograms). The slopes of those distributions are shown for the entire active regions (solid lines) and the HXR sources only (dashed lines).

The MDI magnetograms show that both the SOL2003-04-04T20:55 flare and the SOL2003-10-19T16:50 flare occurred in complex magnetic structures. Although the latter source possesses stronger magnetic fields, the degree of complexity, as represented by the power-law indices, are not much different from each other. However, when

counting only the flare region (as indicated by the circle in top panels), we found the magnetic field distribution in this source to be much lower than any other distributions. The power-law index of 0.44 is close to $\alpha \approx 0.4$, derived from the OVSA spectral analysis. For the C9.0 flare, the 6–12 keV RHESSI sources, constructed at the time interval of 15:58:40 UT–16:02:40 UT, shows two local sources, and therefore, occupy a larger magnetic field region as a whole. The larger power-law index, 0.67, found for the X1.1 flare, implies that the electrons accelerated during this flare gain access to the larger coronal volume, which includes weak fields as well as strong fields. It is plausible that the high-energy electrons are trapped within the large loop found on the EIT images in Fig. 3. The power-law index, 0.67, is higher than $\alpha \approx 0.6$, found in the above spectral analysis of the OVSA data. These indices do not necessarily match the value of α parameter, because α pertains to the corona sources, and the power-law indices derived from the MDI data pertain to the photospheric magnetic fields. Nonetheless, they tend to agree with each other within impressively narrow margins.

5. CONCLUDING REMARKS

In this paper, we explain the motivating ideas of the new analysis tool for solar microwave flux spectra and evaluated its capability for addressing the inhomogeneous magnetic structure of source regions in a quantitative manner. For this purpose, we performed a spectral fitting of two contrasting microwave bursts observed by OVSA, the SOL2003-04-04T20:55 flare with a steep microwave spectrum and the SOL2003-10-19T16:50 flare with a broader spectrum. Our results demonstrate that the stronger event tends to have a higher degree of magnetic inhomogeneity and vice versa, which are supported by the contextual observations of the SOHO EIT images and the MDI magnetograms. We must note that the principle of the proposed method is quite different from imaging-based spectroscopy. Imaging spectroscopy can address the non-uniform distribution of microwave sources on the projected sky-plane but not the inhomogeneous magnetic structure along the line of sight. The spectral analysis tool presented here, on the other hand, provides a systematic way to constrain the magnetic inhomogeneity in both dimensions by employing two parameters that describe how rapidly the coronal magnetic field diverges in 3D space. Another merit is that it is designed for analyzing spatially-integrated flux spectra, which are more common with higher signal-to-noise ratios. This technique is particularly useful for spatially unresolved microwave fluxes observed at multiple frequencies such as those obtained with the Korean Solar Radio Burst Locator (KSRBL; Dou et al. 2009; Hwangbo et al. 2015). In this case, it is more meaningful to seek a range of magnetic fields rather than a single field strength of a microwave source, and quantification of the entire magnetic inhomogeneity is needed. It is also useful for strong flares, which tend to occur in magnetically complex systems, or any limb flares, where the geometrical foreshortening effect limits the source structure from being spatially resolved. Another utility of this simple tool is the ability to rapidly calculate the time-dependent evolution of high-energy electrons from a series of microwave burst spectra, which will be addressed in a companion paper.

ACKNOWLEDGMENTS

We thank Prof. Dale E. Gary at New Jersey Institute of Technology (NJIT) for the OVSA data. JL was supported by the NNSFC grants 41331068, 11790303 (11790300), and 41774180.

REFERENCES

Ai-hua Z, Karlický M, Magnetic field estimation in microwave radio sources, Sol. Phys. 153, 441-444 (1994). https://doi.org/10.1007/BF00712516

Benka SG, Holman GD, A thermal/nonthermal model for solar microwave bursts, Astrophys. J. 391, 854-864 (1992). https://doi.org/10.1086/171394

Brown JC, The temperature structure of chromospheric flares heated by non-thermal electrons, Sol. Phys. 31, 143-169 (1973). https://doi.org/10.1007/BF00156080

Casini R, White SM, Judge PG, Magnetic diagnostics of the solar corona: synthesizing optical and radio techniques, Space Sci. Rev. 210, 145-181 (2017). https://doi.org/10.1007/s11214-017-0400-6

Dou Y, Gary DE, Liu Z, Nita GM, Bong SC, et al., The Korean solar radio burst locator (KSRBL), Publ. Astron. Soc. Pac. 121, 512-526 (2009). https://doi.org/10.1086/599624

Dulk GA, Radio emission from the sun and stars, Ann. Rev. Astron. Astrophys. 23, 169-224 (1985). https://doi.org/10.1146/annurev.aa.23.090185.001125

Dulk GA, Marsh KA, Simplified expressions for the gyrosynchrotron radiation from mildly relativistic, nonthermal and thermal electrons, Astrophys. J. 259, 350-358 (1982). https://doi.org/10.1086/160171

Gary DE, Hurford GJ, Radio spectral diagnostics, in Astrophysics and Space Science Library, Solar and Space Weather

Radiophysics, eds. Gary DE, Keller CU (Springer, Dordrecht, 2004), 71-87.

Holman GD, The effects of low- and high-energy cutoffs on solar flare microwave and hard X-ray spectra, Astrophys. J. 586, 606-616 (2003). https://doi.org/10.1086/367554

Huang G, Calculations of coronal magnetic field parallel and perpendicular to line-of-sight in microwave bursts, Sol. Phys. 237, 173-183 (2006). https://doi.org/10.1007/s11207-006-0097-2

Huang GL, Nakajima H, Diagnosis of coronal magnetic field with data of Nobeyama Radio Heliograph, New Astron. 7, 135-145 (2002). https://doi.org/10.1016/S1384-1076(02)00088-X

Hwangbo JE, Lee J, Park SH, Kim S, Lee DY, et al., Magnetic structure and nonthermal electrons in the X6.9 flare on 2011 august 9, Astrophys. J. 786, 80 (2014). https://doi.org/10.1088/0004-637X/796/2/80

Hwangbo JE, Bong SC, Park SH, Lee DY, Cho KS, et al., Burst locating capability of the Korean solar radio burst locator (KSRBL), J. Astron. Space Sci. 32, 91-99 (2015). http://doi.org/10.5140/JASS.2015.32.1.91

Kosugi T, Denis BR, Kai K, Energetic electrons in impulsive and extended solar flares as deduced from flux, Astrophys. J. 324, 1118-1131 (1988). https://doi.org/10.1086/165967

Kundu MR, Solar Radio Astronomy (John Wiley & Sons Inc., Hoboken, 1965).

Kundu MR, Nindos A, Grechnev VV, The configuration of simple short-duration solar microwave bursts, Astron. Astrophys. 420, 351-359 (2004). https://doi.org/10.1051/0004-6361:20034461

Kuroda N, Gary DE, Wang H, Fleishman GD, Nita GM, et al., Three-dimensional forward-fit modeling of the hard X-ray and microwave emissions of the 2015 june 22 M6.5 flare, Astrophys. J. 852, 32 (2018). https://doi.org/10.3847/1538-4357/aa9d98

Lee J, Electron Transport During Solar Flares, in Astrophysics and Space Science Library, Solar and Space Weather Radiophysics, eds. Gary DE, Keller CU (Springer, Dordrecht, 2004), 179-202.

Lee J, Recent progress in understanding solar magnetic reconnection, J. Astron. Space Sci. 32, 101-112 (2015). https://doi.org/10.5140/JASS.2015.32.2.101

Lee J, Gary DE, Spectral evolution of microwaves and hard X-rays in the 1989 March 18 flare and its interpretation, Sol. Phys. 153, 347-365 (1994). https://doi.org/10.1007/BF00712510

Lee J, Gary DE, Solar Microwave bursts and injection pitch-angle distribution of flare electrons, Astrophys. J. 543, 457-471 (2000). https://doi.org/10.1086/317080

Lee J, Gary DE, Zirin H, Flat microwave spectra seen at X-class flares, Sol. Phys. 152, 409-428 (1994). https://doi.org/10.1007/BF00680447

Lin RP, Dennis BR, Hurford GJ, Smith DM, Zehnder A, The Reuven Ramaty high-energy solar spectroscopic imager (RHESSI), Sol. Phys. 210, 3-32 (2002). https://doi.org/10.1023/A:1022428818870

Melrose DB, Plasma Astrophysics (Gordon and Breach Science Pubilshers, New York, 1980).

Moschou SP, Sokolov I, Cohen O, Drake JJ, Borovikov D, Synthetic radio imaging for quiescent and CME-flare scenarios, Astrophys. J. 867, 51 (2018). https://doi.org/10.3847/1538-4357/aae58c

Nindos A, White SM, Kundu MR, Gary DE, Observations and models of a flaring loop, Astrophys. J. 533, 1053-1062 (2000). https://doi.org/10.1086/308705

Nita GM, Fleishman GD, Kuznetsov AA, Kontar EP, Gary DE, Three-dimensional radio and X-ray modeling and data analysis software: revealing flare complexity, Astrophys. J. 799, 236 (2015). https://doi.org/10.1088/0004-637X/799/2/236

Powell KG, Roe PL, Linde TJ, Gombosi TI, De Zeeuw DL, A Solution-Adaptive Upwind Scheme for Ideal Magnetohydrodynamics, J. Comput. Phys. 154, 284-309 (1999). https://doi.org/10.1006/jcph.1999.6299

Ramaty R, Gyrosynchrotron emission and absorption in a magnetoactive plasma, Astrophys. J. 158, 753-770 (1969). https://doi.org/10.1086/150235

Raulin JP, White SM, Kundu MR, Silva AVR, Shibasaki K, Multiple Components in the Millimeter Emission of a Solar Flare, Astrophys. J. 522, 547-558 (1999). https://doi.org/10.1086/322974

Rybicki GB, Lightman AP, Radiative processes in astrophysics (John Wiley & Sons Inc., Hoboken, 1985).

Song QW, Nakajima H, Huang GL, Tan BL, Huang Y, et al., Turnover frequency in solar microwave bursts with an extremely flat optically thin spectrum, Sol. Phys. 291, 3619-3635 (2016). https://doi.org/10.1007/s11207-016-1004-0

Trottet G, Raulin JP, Giménez de Castro G, Lüthi T, Caspi A, et al., Origin of the Submillimeter Radio Emission During the Time-Extended Phase of a Solar Flare, Sol. Phys, 273, 339-361 (2011). https://doi.org/10.1007/s11207-011-9875-6

Zheleznyakov VV, Radio emission of the sun and planets (Pergamon Press, Oxford, 1970).